Respiratory Medicine 155 (2019) 79–85

Contents lists available at ScienceDirect

Respiratory Medicine

journal homepage: www.elsevier.com/locate/rmed

Review article

Magnetic resonance imaging of interstitial lung diseases: A state-of-the-art review

Lilian Lonzetti[a], Matheus Zanon[b], Gabriel Sartori Pacini[b], Stephan Altmayer[b,c], Diogo Martins de Oliveira[c], Adalberto Sperb Rubin[d], Fernando Ferreira Gazzoni[b], Marcelo Cardoso Barros[b,c,d], Bruno Hochhegger[b,c,d,*]

[a] Department of Rheumatology, Irmandade Santa Casa de Misericórdia de Porto Alegre, Porto Alegre, R. Sarmento Leite, 245, 90050-170, Brazil
[b] Medical Imaging Research Lab, LABIMED, Department of Radiology, Pavilhão Pereira Filho Hospital, Irmandade Santa Casa de Misericórdia de Porto Alegre, Porto Alegre, Av. Independência, 75, 90020160, Brazil
[c] School of Medicine, Postgraduate Program in Medicine and Health Sciences, Pontifícia Universidade Católica do Rio Grande do Sul, Porto Alegre, Av. Ipiranga, 6681, 90619-900, Brazil
[d] Department of Pulmonology, Pavilhão Pereira Filho Hospital, Irmandade Santa Casa de Misericórdia de Porto Alegre, Porto Alegre, Av. Independência, 75, 90020160, Brazil

ARTICLE INFO

Keywords:
Interstitial lung disease
Computed tomography
Magnetic resonance imaging
Idiopathic pulmonary fibrosis
Connective tissue disease
Sarcoidosis

ABSTRACT

Magnetic resonance imaging (MRI) has been emerging as an imaging modality to assess interstitial lung diseases (ILD). An optimal chest MRI protocol for ILDs should include non-contrast breath-holding sequences, steady-state free-precession sequences, and contrast-enhanced sequences. One of the main MRI applications in ILDs is the differentiation between areas of active inflammation (i.e. reversible stage) and fibrosis. Alveolitis presents high signal intensity on T2-weighted sequences (WS) and early-enhancement on contrast-enhanced MR sequences, while fibrotic-predominant lesions present low signal and late-enhancement in these sequences, respectively. MRI can be useful in connective tissue diseases, idiopathic pulmonary fibrosis, and sarcoidosis. The aim of this state-of-the-art review was to perform a state-of-the-art review on the use of MRI in ILDs, and propose the optimal MRI protocols for imaging ILDs.

1. Introduction

Interstitial lung diseases (ILD) are a heterogeneous group of disorders characterized by diffuse damage of the lung parenchyma, affecting mainly the most peripheral and delicate interstitium in the alveolar walls [1–3]. There are more than 200 ILDs described, including infectious, immunologic, environmental, toxic and genetic mechanisms, whereas an etiological agent cannot be identified in many ILDs [1–4].

Diffuse ILDs mostly encompass inflammatory processes of the lung interstitium, which comprehends the space between the epithelial and endothelial basement membranes [1,4–6]. However, these disorders frequently affect not only the interstitium, but the airspaces, peripheral airways, and vessels along with their respective epithelial and endothelial linings [5,6]. A repeated injury may lead to progressive interstitial fibrosis, either in the form of abnormal collagen deposition or proliferation of fibroblasts capable of collagen synthesis [1,7]. Regardless of the underlying etiology, lung fibrosis is considered an irreversible process, representing a cardinal feature of many ILDs [4–6]. Significant pulmonary fibrosis compromises respiratory function and may lead to respiratory failure and death if the injury continues with progressive amount of fibrosis.

Computed tomography (CT) has been the gold standard imaging method for ILDs evaluation. As clinical presentation and histopathologic patterns can show significant overlap in ILDs, and significant heterogeneity of disease throughout the lung may be present, chest CT is considered critical tool in the initial evaluation of ILDs [8,9]. However, CT is associated with ionizing radiation exposure, what should be a concern especially for patients with ILD as multiple CT scans might be necessary through the chronic course of these pathologies.

With recent technical developments, magnetic resonance imaging

* Corresponding author. Professor of Radiology Institutional affiliation: Federal University of Health Sciences of Porto Alegre, R. Sarmento Leite, 245, Porto Alegre, 90050-170, Brazil.
E-mail addresses: lilianlonzetti@hotmail.com, brunohochhegger@gmail.com (L. Lonzetti), mhgzanon@hotmail.com (M. Zanon), gabrielsartorip@gmail.com (G.S. Pacini), stephanaltmayer@gmail.com (S. Altmayer), oliveira.diogo1@hotmail.com (D. Martins de Oliveira), arubin@terra.com.br (A.S. Rubin), gazzoni4@gmail.com (F.F. Gazzoni), macardosob@gmail.com (M.C. Barros), brunoho@ufcspa.edu.br (B. Hochhegger).

https://doi.org/10.1016/j.rmed.2019.07.006
Received 10 April 2019; Received in revised form 31 May 2019; Accepted 5 July 2019
Available online 06 July 2019

(MRI) has been emerging as an imaging modality to assess the chest. Combining functional and morphological information, MRI has been arising as a radiation-free alternative, comparable to CT in many instances [10,11]. However, evidence available in the literature is weak for the use of MRI in the assessment of ILD [12]. The aim of this study was to perform a state-of-the-art review on the main applications of MRI in ILD, and discuss the optimal MRI protocols for evaluating these diseases.

2. Chest MRI protocol

A standard chest MRI protocol is mainly based on non-contrast breath-holding sequences and takes approximately 15 min [13]. The imaging protocol usually begins with a gradient echo (GRE) localizer during inspiration (two-dimensional fast low-angle shot, 2D-FLASH). After this localizer sequence, a coronal T2-weighted is usually the first sequence to be acquired using single shot techniques (e.g., Half-Fourier Acquisition Single-shot Turbo spin Echo imaging, HASTE, by Siemens; Single-shot fast spin echo, SS-FSE, by General Electrics, GE) [13,14]. T2-weighted HASTE is useful to demonstrate pulmonary infiltrates, mucus and fluid accumulation and inflammatory bronchial thickening. Air-space infiltrates are demonstrated as hyperintense areas on the T2-weighted images contrasting against the dark background of the normal lung parenchyma [11]. Fast T2-weighted spin-echo sequences with respiratory triggering are a reasonable alternative to patients that cannot cooperate or breath-hold [15–17]. Following T2-HASTE, a transverse T1-weighted sequence is obtained using spoiled three-dimensional (3D) GRE (e.g., volumetric interpolated breath-hold examination, VIBE, by Siemens). T1-3D-GRE is helpful for the evaluation of pulmonary nodules, masses, consolidations, and mediastinum [13]. However, T1-GRE images do not provide enough information about infiltrative processes for diagnostic purposes [14].

Afterwards, a steady-state free-precession GRE sequence may be acquired during free breathing (e.g., true fast imaging with steady-state precession, TrueFISP, by Siemens; fast imaging employing steady-state acquisition, FIESTA, by GE; balanced fast field echo, balanced-FFE, by Philips). Steady-state free-precession acquisitions have advantage over some single-shot fast spin echo sequences, such as HASTE, due to shorter echo and acquisition times, lower sensitivity to motion artefacts and mixed T2/T1 contrast weighting [18]. In a study that used a two-dimensional balanced steady-state free-precession sequence, MRI revealed a sensitivity of 89% in the identification of pulmonary fibrosis, depicting 75% of ground-glass opacities, 67% of traction bronchiectasis and 45% of cystic fibrosis [18]. TrueFISP sequences also can display lung vessels with excellent contrast, and several studies have demonstrated a great accuracy in the detection of pulmonary embolism [19–22]. As patients with ILDs are at higher risk for PE, the inclusion of a steady-state sequence is recommended [23,24].

The standard protocol can be extended to included contrast-enhanced sequences. Post-contrast scans markedly improve the diagnostic yield of 3D-GRE sequences by clearer visualization of vascular and hilar structures, pleura, and solid nodules/masses. Contrast-enhanced images are also helpful to characterize lung fibrosis represented by late-enhancement areas in T1-weighted 3D-GRE acquisitions from 1 to 10 min after contrast administration [6,25–27]. T1-weighted 3D-GRE sequences with the use of parallel imaging and echo sharing allow for short acquisition times of approximately 1.5s for a 3D dataset (so-called 4D or 3D + t) needed to visualize perfusion during the peak enhancement of the lung parenchyma [13].

In patients with ILDs at moderate-advanced stages, breath-hold might be problematic, and some techniques to prolong breath-hold may be necessary, such as the use of nasal canulla for oxygen delivery, hyperventilation of the patient before sequence acquisition, and reduction in the number of phase encoding steps of the sequence [27]. Parallel imaging techniques are recommended as they allow substantial improvement in image acquisition speed by using arrangements of multiple coils to acquire additional information along the phase encoding direction [13,14]. When parallel imaging techniques are not available, multi-breath hold acquisitions can be used instead. ECG is not required on a routine basis, but ECG-triggered sequences can be planned when it is necessary to enhance details of structures close to the heart. Half-Fourier acquisition or ultra-short echo times (UTE) are recommended [28]. UTE sequences can limit signal decay and produce high signal-to-noise and high-resolution images. Using a UTE of 192 μs, Ohno and colleagues found an excellent diagnostic performance of MRI in the identification of ILD and/or pulmonary fibrosis, with no significant difference compared to standard or low-dose CT [29].

Another sequence using UTE that has been investigated for chest MRI is the pointwise encoding time reduction with radial acquisition (PETRA) sequence, which is a noiseless prototype hybrid approach to UTE three-dimensional imaging capable of achieving the shortest possible encoding time for a given imaging unit [30,31]. Dournes et al. investigated the use of PETRA sequence with respiratory gating in healthy lung MR imaging compared to conventional T1-weighted VIBE and found significant differences in the visibility of fine lung structures, such as lung fissures, bronchi, and small vessels [31]. Despite significantly higher cardiac and respiratory motion artefacts with PETRA, all bronchi could be visualized up to the sub-segmental generation in this sequence, whereas conventional VIBE segmental could only identify all bronchi up to the lobar generation [31]. The authors also included three patients with cystic fibrosis and found a 100% agreement between the CT and PETRA-MR images, despite motion artefacts due to moderate-severe dyspnea [31]. However, till now, the PETRA sequence has not been investigated in ILD.

Chest magnetic resonance elastography (MRE) is another technique that has also been studied as a promising biomarker of ILDs. This non-invasive technique can quantify the topographical distribution of shear stiffness in tissues and is already widely used in the assessment of liver fibrosis [32]. In a study by Marineli et al., MRE could quantitatively differentiate healthy controls and patients with ILDs, as the parenchymal shear stiffness was increased in fibrotic zones of the lung at both the residual volume and the total lung capacity (Fig. 1) [33].

3. Evaluation of inflammation and fibrosis predominant lesions

Many ILD have a clinical course characterized by an alternation of acute exacerbations and chronic stable disease, with variable degrees of inflammation and fibrosis [1,6,25]. Differentiation of inflammation and fibrosis-predominant lesions is important to predict prognosis of ILDs which could determine specific target-treatments. The presence of alveolitis in ILDs, a marker of active disease, could predict response to treatment with immunosuppressive or anti-inflammatory drugs, while fibrotic changes are irreversible. At high-resolution CT, areas of active inflammation and fibrosis can have similar patterns, presenting as ground-glass opacities for example, and lung biopsy might be required.

Usually, lesions with high metabolic activity, such as inflammation and tumors, are associated with high water content within the tissues. For this reason, active alveolitis could be demonstrated on T2-weighted MRI as areas of high signal, whereas fibrotic-predominant lesions would present a low signal (Figs. 1 and 2). The presence of high signal intensity lesions has been reported as a helpful predictor of treatment response and prognosis [34].

Contrast-enhanced MRI sequences are also useful in the evaluation of ILDs. In previous series, early-enhanced lesions were an accurate indicator of active disease, while late-enhancement was a characteristic of fibrotic-predominant lesions [25,27,35]. Molecules of gadolinium can freely diffuse across the capillary's endothelium into the extravascular spaces of lung interstitium and later reenter the intravascular space [36,37]. Inflammatory-predominant lesions present an increased extravascular interstitium volume and increased angiogenesis, what would explain the earlier and faster enhancement on MR images compared to normal lung interstitium [25]. On the other hand, late-

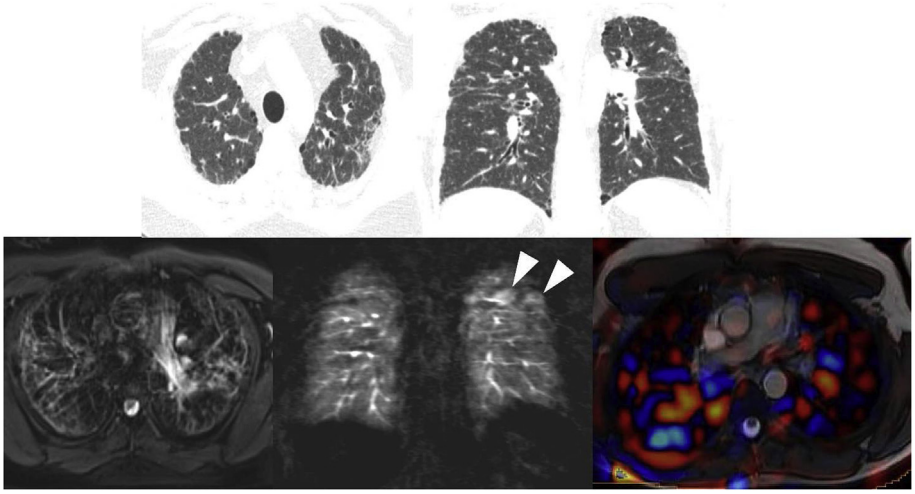

Fig. 1. 61-year-old woman with non-specific interstitial pneumonia. high-resolution CT (HRCT) axial (A) and coronal (B) images demonstrate diffuse reticulation and traction bronchiectasis, and mild ground-glass opacities in the left upper lobe. In the MRI, the corresponding areas of ground-glass opacities are seen as hyperintense lesions in the axial T2-weighted sequence (C). In the T1-weighted post-gadolinium sequence, these areas demonstrate an early enhancement (arrowheads) in the early acquisitions (D) most likely zones of active inflammation, which were further confirmed through left upper lobe biopsy. Combined MRI magnitude and elastogram axial images (E) demonstrate an increased parenchymal shear stiffness in the areas of fibrosis.

enhancement associated with fibrotic-predominant lesions might be a result of the destruction of the lung interstitium microvasculature due to fibrosis, impairing contrast washout (Fig. 3). In a recent proof-of-concept study, Lavelle et al. tested a segmented inversion-recovery turbo low-angle shot MRI sequence (turboFLASH) to evaluate lung fibrosis, adjusting the inversion times individually to null the blood pool in the pulmonary artery, hence nulling the signal from contrast within the pulmonary circulation. They found significantly higher late-enhanced MRI signal for lung fibrosis, presenting a 204.8% higher signal compared to the normal lung [27].

4. Magnetic resonance imaging in specific interstitial lung diseases

4.1. Connective tissue diseases

Several connective tissue diseases (CTD) can course with lung involvement, such as systemic lupus erythematosus, rheumatoid arthritis, systemic sclerosis, Sjogren syndrome, dermatomyositis, polymyositis, and mixed connective tissue disease [38,39]. ILD usually is the most common pulmonary complication in CTD and can be the first complication of these diseases, preceding in years other manifestations [38,39].

Parenchymal pulmonary abnormalities found in CTD-related ILDs (CTD-ILD) are classified with the same pathologic-radiologic system than other ILD [40]. Non-specific interstitial pneumonia (NISP) and usual interstitial pneumonia (UIP) are the most common patterns described in patients with CTD-ILD [41]. In NISP, both interstitial inflammation and fibrosis can occur at the same time [42] (Fig. 4). MRI has also been shown to accurately detect inflammation areas within lung tissue of patients with systemic sclerosis with great agreement with CT findings [43] (Fig. 5). In a study by Pinal-Fernandez et al., MRI presented an area under the curve of 0.96 to detect ILD in systemic sclerosis, also presenting good intra- and inter-reader agreement and good significant correlations to forced vital capacity, diffusing capacity of carbon monoxide, and HRCT [44].

The use of quantitative MR imaging in patients with CTD-related ILD has also been investigated. In a 3T scanner, Ohno et al. used echo times lower than 100 μs, minimizing the signal decay due to short transverse relaxation time (T2/T2 star [T2*]) [42]. The authors found significantly higher T2* values in patients with CTD-ILD compared to normal controls with significant correlations to pulmonary function tests and serum levels of KL-6 (a marker of pneumonitis) [42]. These results suggested that quantitative MRI might be as effective as thin-section CT for assessment of disease severity in terms of pulmonary involvement in CTD patients [42]. In a study by this same research group, the authors also found oxygen-enhanced MRI to be as useful as thin-section CT for pulmonary functional loss and disease severity assessment of CTD patients with ILD [45].

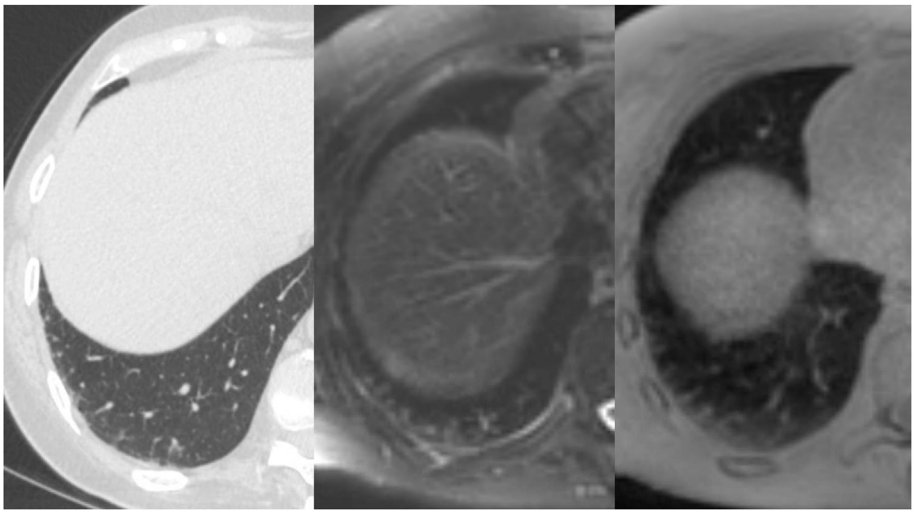

Fig 2. 47-year-old man with rheumatoid arthritis. High-resolution CT image (A) shows mild subpleural interlobular septal thickening. T2-weighted MRI (B) shows mild hyperintense areas along with the subpleural interlobular septal thickening, which were further confirmed as active inflammation in histopathology. These findings could also be seen in the PETRA sequence (C), despite the known limitation of this MRI sequence in susceptible areas to respiratory motion, such as the lung bases.

Fig 3. 64-year-old man with idiopathic pulmonary fibrosis. CT axial image (A) and T1-weighted VIBE post-gadolinium images (B) demonstrate late enhancement in the subpleural zones of lung fibrosis.

4.2. Idiopathic pulmonary fibrosis

The most common form of idiopathic interstitial pneumonia is idiopathic pulmonary fibrosis (IPF). The main imaging modality in IPF is HRCT which plays an essential role in the initial assessment of suspected IPF, considerably influencing subsequent management decisions. The primary role of HRCT is to distinguish chronic fibrosing lung diseases with a UIP pattern from those presenting a non-UIP pattern, suggesting an alternative diagnosis when possible [46]. The presence of a typical UIP pattern on HRCT in the absence of any evidence for an alternative etiology for the ILD is enough for the diagnosis of IPF [47]. In the absence of a typical UIP CT pattern, surgical lung biopsy is advised for the final diagnosis [47]. However, lung biopsy is an invasive procedure, and associated mortalities rates from 2% to 7.1% have been reported in ILDs [48,49].

Thus far, evidence on the use of chest MR imaging in IPF is weak [50]. Some studies have investigated MRI as a complementary tool to HRCT that could possibly provide more data to obviate the need for invasive diagnostic procedures. A case with typical UIP HRCT pattern and the corresponding MR images demonstrating the honeycombing and reticulation is shown in Fig. 6. In a series with patients with pathologically proven UIP and nonspecific interstitial pneumonia (NSIP), quantitative MRI findings were able to differentiate active-inflammatory and stable-fibrotic lesions in NSIP [26]. In NSIP, patients with suspected inflammatory activity presented significantly higher T2 relaxation times and proton density values than those with stable disease. However, these parameters were not able to differentiate UIP and NSIP individually, and the only significant difference between these

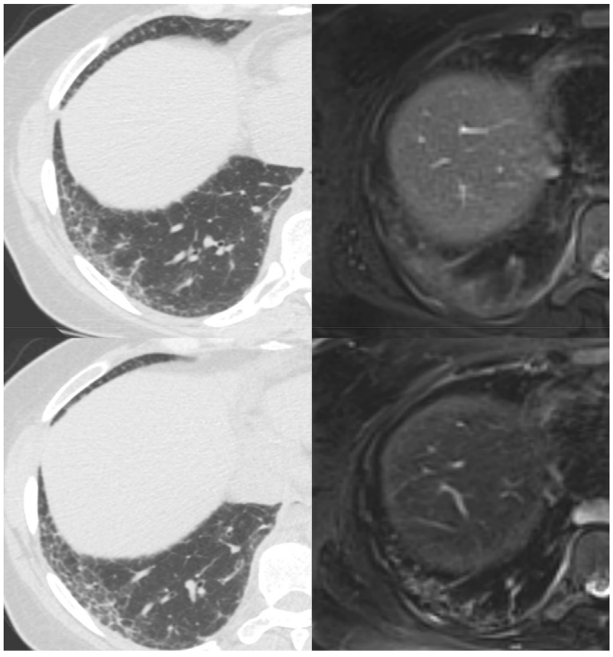

Fig 4. 58-year-old man with CTD-related ILD. HRCT axial image (A) demonstrates a probable usual interstitial pneumonia pattern with subpleural reticulation and traction bronchiectasis. T2-weighted BLADE image (B) shows areas of hyperintensity in the right lower lobe, which were confirmed as inflammatory lesions in histopathology. After a three-month course of anti-inflammatory drugs, the findings remain mostly unaltered in the HRCT control scan (C), while in the MRI control scan (D) the hyperintense areas previously seen are resolved.

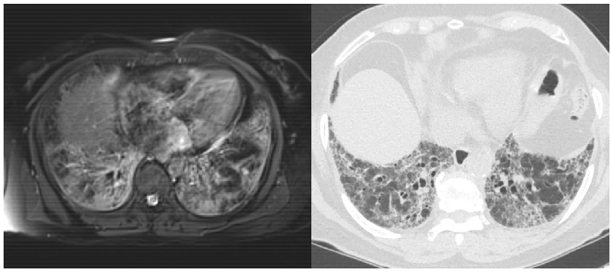

Fig 5. 80-year-old woman with systemic sclerosis. Active-inflammatory biopsy-confirmed pulmonary lesions in the lower lobes presenting hyperintensity in T2-weighted BLADE MRI (A) and ground-glass opacities in the HRCT scan (B).

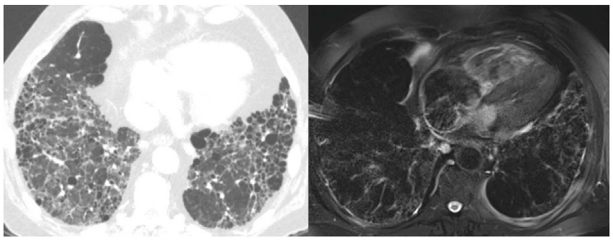

Fig 6. 61-year-old man with idiopathic pulmonary fibrosis. HRCT axial image (A) shows a typical usual interstitial pneumonia pattern with reticular opacities with subpleural and basal predominance and honeycombing. The corresponding T2-weighted MRI (B) also shows the same findings. Note that it is not possible to find any hyperintense active-inflammatory lesion that could represent a reversible stage of the disease.

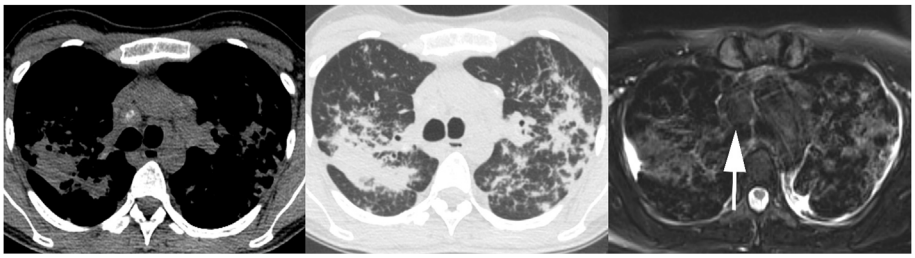

Fig 7. 42-year-old woman with pulmonary sarcoidosis. Non-contrast HRCT axial images (A and B) show reticulation, nodules, masses, and mediastinal lymphadenopathy. The same findings can be seen as hyperintense areas in T2-weighted BLADE (C). The enlarged calcified lymph node located in the right lower paratracheal station presents a hypointense core with a thin rim of hyperintensity in the T2-weighted MRI (arrow), characterizing the "dark lymph node sign".

two patterns on proton densities was for advanced lesions with dorsal location [26]. The authors hypothesized that air-containing cystic lesions in UIP such as honeycombing would contribute to a lower proton density in a dorsal distribution of the lungs.

A promising modality that can reveal subtle changes in lung ventilation and microstructure is MRI with hyperpolarized gases, such as helium (^{3}He MRI) or xenon (^{129}Xe MRI) [51]. Historically, one of the major drawbacks of lung MRI has been the much lower density of hydrogen protons in the lungs compared to other anatomical structures, limiting the signal available for MRI. Hyperpolarization of external gases, such as ^{3}He and ^{129}Xe, increase their magnetization, allowing them to work as gaseous contrast media to image the airways and airspaces [52]. Although ^{3}He MRI has been studied for diseases such as chronic obstructive pulmonary disease, asthma, and cystic fibrosis, the use of ^{3}He MR imaging is not economically sustainable due to ^{3}He low availability and high costs, with prices per liter varying from $800 to $2000 [52–56]. On the other hand, MRI hyperpolarized with ^{129}Xe has been demonstrated to be a well-tolerated and fast technique, allowing evaluation of the gas uptake in the microstructures of the lungs. ^{129}Xe present different resonance frequency shifts for every tissue it crosses through diffusion in the alveoli (alveolar epithelial cells, interstitial tissues, capillary endothelium, plasma, and capillary red blood cells (RBC)), which can be measured on MR spectroscopy [52,57–59]. Due to these proprieties, ^{129}Xe MRI has been studied for IPF assessment, providing both structural and functional information on fibrotic change and gas exchange [60–62]. In a study by Wang et al., the authors found that the ratio of the signal from the ^{129}Xe uptake in RBCs by the signal of the gas uptake in the alveoli barrier was significantly reduced in patients with IPF, reflecting interstitial thickening and poor gas transfer to RBCs [61]. Moreover, the ^{129}Xe indices were correlated to monoxide carbon diffusion factor (DLco), a direct marker of global gas exchange used in the assessment of ILDs, suggesting that both techniques reflect similar underlying gas exchange pathophysiology RBCs [61]. Likewise, Weatherley et al. also found similar correlations, sensitive to longitudinal changes in IPF in a follow-up period of 12 months, demonstrating that ^{129}Xe MR spectroscopy maybe could be useful for diagnosing and monitoring IPF disease progression [62].

4.3. Sarcoidosis

Sarcoidosis is an inflammatory autoimmune multisystemic condition with diffuse collections of noncaseating granulomas throughout the body. In most cases, the disease affects the lungs (> 90% of patients) and the lymphatic system (about one-third of cases) [63,64]. The diagnosis of sarcoidosis is usually done as a diagnosis of exclusion when no other identifiable cause of granulomatous inflammation can be found, such as mycobacterial and atypical mycobacterial disease and some lung mycoses, such as coccidioidomycosis and histoplasmosis [65]. Non-caseating granulomas with epithelioid and giant cells are the histological hallmark of sarcoidosis [64,65]. On imaging, pulmonary sarcoidosis usually presents as perilymphatic nodularity commonly with symmetric hilar and mediastinal lymphadenopathy, and in chronic cases, lung involvement can progress to fibrosis [64,66,67]. HRCT is one of the main imaging modalities in sarcoidosis, as it is the standard for assessment of pulmonary findings, lung fibrosis, and mediastinal lymph nodes [66,67]. HRCT presents better efficacy in assessing subtle parenchymal modifications even in the early stages of sarcoidosis that may be unnoticed in chest radiographies [66,67].

As sarcoidosis is a chronic disease with an early onset age, between 25 and 40 years, many patients will undergo several imaging investigations, raising concerns on cumulative exposure to ionizing radiation [63,64]. As a radiation-free alternative, chest MRI applications in sarcoidosis have been widened in the previous years. Studies have reported a good correlation between MRI and HRCT in pulmonary sarcoidosis [66,68,69]. In a study by Chung et al., MRI was comparable to HRCT in the assessment of parenchymal opacification and reticulation in sarcoidosis [66] (Fig. 7). However, MRI sensitivity for nodules evaluation and fine reticulation was lower, a limitation that might have occurred due to the inherent lower spatial resolution of MRI and the acquisition protocol adopted in the study, non-optimal for nodules assessment on MRI [13,66,70]. In a study using late-enhanced chest MRI with individual nulling of the pulmonary blood pool signal (turbo-FLASH sequence), MRI could detect and determine the extension of fibrotic pulmonary sarcoid, accurately comparing to the anatomical characterization on HRCT [69].

Another advantage is that MRI can accurately detect subtle enhancement and necrosis within mediastinal and hilar lymphadenopathy (Fig. 8). Presence of necrosis within mediastinal and hilar lymph nodes is a feature commonly found in tuberculosis but not in sarcoidosis, what can help in the differential diagnosis [67]. A characteristic MRI appearance of lymphadenopathy in sarcoidosis has been described in the literature as the "dark lymph node sign" [71]. This feature represents hilar and mediastinal lymph nodes with an internal hypointensity and peripheral rim of hyperintensity on T2-FSE (BLADE) and post-gadolinium 3D-GRE (VIBE) images (Fig. 7). The dark lymph node sign was present in up to 49% of patients with sarcoidosis and probably corresponds to areas of central nodal fibrosis [71].

5. Summary

In this state-of-the-art review, we have discussed several applications of MRI in the evaluation of interstitial lung diseases, such as CTD, IPF, and sarcoidosis. Despite still being mostly restricted to research purposes, the field of use of MRI in thoracic imaging continuously increases with recent improvements of acquisition techniques and

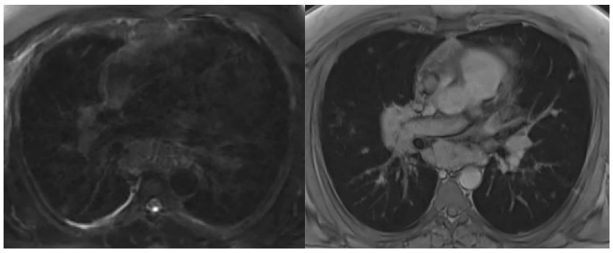

Fig 8. 37-year-old man with pulmonary sarcoidosis. MR images show enlarged lymph nodes in the subcarinal and hilar regions, presenting low signal intensity in T2-weighted BLADE (A) and prominent homogeneous enhancement in T1-weighted VIBE post-gadolinium (B).

imaging resolution. Although more robust evidence is needed, MRI will very likely start to be featured in the management of interstitial lung diseases.

Conflicts of interest

None.

Declarations of interest

None.

Ethical approval

This article does not contain any studies with human participants or animals performed by any of the authors.

Funding

None.

Acknowledgments

None.

References

[1] V. Kumar, A.K. Abbas, J.C. Aster, Robbins basic pathology e-book, Elsevier Health Sciences, 2017.
[2] K. Junker, F. Brasch, Interstitial lung diseases, Pathologe 29 (2008) 273–279.
[3] K.M. Antoniou, G.A. Margaritopoulos, S. Tomassetti, F. Bonella, U. Costabel, V. Poletti, Interstitial lung disease, Eur. Respir. Rev. 23 (131) (2014) 40–54.
[4] K.O. Leslie, Pathology of interstitial lung disease, Clin. Chest Med. 25 (4) (2004) 657–703.
[5] W.D. Travis, T.E. King, E.D. Bateman, D.A. Lynch, F. Capron, D. Center, et al., American Thoracic Society/European Respiratory Society international multidisciplinary consensus classification of the idiopathic interstitial pneumonias, Am. J. Respir. Crit. Care Med. 165 (2) (2002) 277–304.
[6] G. Lutterbey, C. Grohé, J. Gieseke, M. von Falkenhausen, N. Morakkabati, M. Wattjes, et al., Initial experience with lung-MRI at 3.0 T: comparison with CT and clinical data in the evaluation of interstitial lung disease activity, Eur. J. Radiol. 61 (2) (2007) 256–261.
[7] D.W. Visscher, J.L. Myers, Histologic spectrum of idiopathic interstitial pneumonias, Proc. Am. Thorac. Soc. 3 (4) (2006) 322–329.
[8] B. Elicker, C.A. de Castro Pereira, R. Webb, K.O. Leslie, Padrões tomográficos das doenças intersticiais pulmonares difusas com correlação clínica e patológica, J. Bras. Pneumol. 34 (9) (2008) 715–744.
[9] K. Leslie, My approach to interstitial lung disease using clinical, radiological and histopathological patterns, J. Clin. Pathol. 62 (5) (2009) 387–401.
[10] J. Wild, H. Marshall, M. Bock, L. Schad, P. Jakob, M. Puderbach, et al., MRI of the lung (1/3): methods, Insights into imaging 3 (4) (2012) 345–353.
[11] J. Biederer, S. Mirsadraee, M. Beer, F. Molinari, C. Hintze, G. Bauman, et al., MRI of the lung (3/3)—current applications and future perspectives, Insights into Imaging 3 (4) (2012) 373–386.
[12] C. Romei, L. Turturici, L. Tavanti, J. Miedema, S. Fiorini, M. Marletta, et al., The use of chest magnetic resonance imaging in interstitial lung disease: a systematic review, Eur. Respir. Rev. 27 (150) (2018) 180062.
[13] B. Hochhegger, VVSd Souza, E. Marchiori, K.L. Irion, A.S. Souza Jr., J. Elias Junior, et al., Chest magnetic resonance imaging: a protocol suggestion, Radiol. Bras. 48 (6) (2015) 373–380.
[14] M. Puderbach, C. Hintze, S. Ley, M. Eichinger, H.-U. Kauczor, J. Biederer, MR imaging of the chest: a practical approach at 1.5 T, Eur. J. Radiol. 64 (3) (2007) 345–355.
[15] J. Biederer, I. Busse, J. Grimm, M. Reuter, C. Muhle, S. Freitag, et al., Sensitivity of MRI in detecting alveolar infiltrates: experimental studies, Röfo: Fortschritte dem Geb. Rontgenstrahlen Nukl. 174 (8) (2002) 1033–1039.
[16] C. Leutner, H. Schild (Eds.), MRT des Lungenparenchyms. RöFo-Fortschritte auf dem Gebiet der Röntgenstrahlen und der bildgebenden Verfahren, © Georg Thieme Verlag Stuttgart·, New York, 2001.
[17] M. Both, J. Schultze, M. Reuter, B. Bewig, R. Hubner, I. Bobis, et al., Fast T1-and T2-weighted pulmonary MR-imaging in patients with bronchial carcinoma, Eur. J. Radiol. 53 (3) (2005) 478–488.
[18] S. Rajaram, A.J. Swift, D. Capener, A. Telfer, C. Davies, C. Hill, et al., Lung morphology assessment with balanced steady-state free precession MR imaging compared with CT, Radiology 263 (2) (2012) 569–577.
[19] L. Pasin, M. Zanon, J. Moreira, A.L. Moreira, G. Watte, E. Marchiori, et al., Magnetic resonance imaging of pulmonary embolism: diagnostic accuracy of unenhanced MR and influence in mortality rates, Lung 195 (2) (2017) 193–199.
[20] W. Hosch, M. Schlieter, S. Ley, T. Heye, H.-U. Kauczor, M. Libicher, Detection of acute pulmonary embolism: feasibility of diagnostic accuracy of MRI using a stepwise protocol, Emerg. Radiol. 21 (2) (2014) 151–158.
[21] M.P. Revel, O. Sanchez, C. Lefort, G. Meyer, S. Couchon, A. Hernigou, et al., Diagnostic accuracy of unenhanced, contrast-enhanced perfusion and angiographic MRI sequences for pulmonary embolism diagnosis: results of independent sequence readings, Eur. Radiol. 23 (9) (2013) 2374–2382.
[22] B. Kalb, P. Sharma, S. Tigges, G.L. Ray, H.D. Kitajima, J.R. Costello, et al., MR imaging of pulmonary embolism: diagnostic accuracy of contrast-enhanced 3D MR pulmonary angiography, contrast-enhanced low–flip angle 3D GRE, and nonenhanced free-induction FISP sequences, Radiology 263 (1) (2012) 271–278.
[23] G.A. Margaritopoulos, K.M. Antoniou, A.U. Wells, Comorbidities in interstitial lung diseases, Eur. Respir. Rev. 26 (143) (2017) 160027.
[24] D.B. Sprunger, A.L. Olson, T.J. Huie, E.R. Fernandez-Perez, A. Fischer, J.J. Solomon, et al., Pulmonary fibrosis is associated with an elevated risk of thromboembolic disease, Eur. Respir. J. 39 (1) (2012) 125–132.
[25] C.A. Yi, K.S. Lee, J. Han, M.P. Chung, M.J. Chung, K.M. Shin, 3-T MRI for differentiating inflammation-and fibrosis-predominant lesions of usual and nonspecific interstitial pneumonia: comparison study with pathologic correlation, Am. J. Roentgenol. 190 (4) (2008) 878–885.
[26] M.T. Buzan, A. Wetscherek, C.P. Heussel, M. Kreuter, F.J. Herth, A. Warth, et al., Texture analysis using proton density and T2 relaxation in patients with histological usual interstitial pneumonia (UIP) or nonspecific interstitial pneumonia (NSIP), PLoS One 12 (5) (2017) e0177689.
[27] L.P. Lavelle, D. Brady, S. McEvoy, D. Murphy, B. Gibney, A. Gallagher, et al., Pulmonary fibrosis: tissue characterization using late-enhanced MRI compared with unenhanced anatomic high-resolution CT, Diagn. Interventional Radiol. 23 (2) (2017) 106.
[28] B. Hochhegger, E. Marchiori, K. Irion, Acute pulmonary embolism, N. Engl. J. Med. 363 (20) (2010) 1972.
[29] Y. Ohno, H. Koyama, T. Yoshikawa, S. Seki, D. Takenaka, M. Yui, et al., Pulmonary high-resolution ultrashort TE MR imaging: comparison with thin-section standard-and low-dose computed tomography for the assessment of pulmonary parenchyma diseases, J. Magn. Reson. Imaging 43 (2) (2016) 512–532.
[30] D.M. Grodzki, P.M. Jakob, B. Heismann, Ultrashort echo time imaging using pointwise encoding time reduction with radial acquisition (PETRA), Magn. Reson. Med. 67 (2) (2012) 510–518.
[31] G. Dournes, D. Grodzki, J. Macey, P.-O. Girodet, M. Fayon, J.-F. Chateil, et al., Quiet submillimeter MR imaging of the lung is feasible with a PETRA sequence at 1.5 T, Radiology 276 (1) (2015) 258–265.
[32] Y.K. Mariappan, K.J. Glaser, R.D. Hubmayr, A. Manduca, R.L. Ehman, K.P. McGee, MR elastography of human lung parenchyma: technical development, theoretical modeling and in vivo validation, J. Magn. Reson. Imaging 33 (6) (2011) 1351–1361.
[33] J.P. Marinelli, D.L. Levin, R. Vassallo, R.E. Carter, R.D. Hubmayr, R.L. Ehman, et al., Quantitative assessment of lung stiffness in patients with interstitial lung disease using MR elastography, J. Magn. Reson. Imaging 46 (2) (2017) 365–374.
[34] N. Müller, J. Mayo, C. Zwirewich, Value of MR imaging in the evaluation of chronic infiltrative lung diseases: comparison with CT, AJR Am. J. Roentgenol. 158 (6) (1992) 1205–1209.
[35] M. Gaeta, A. Blandino, E. Scribano, F. Minutoli, M. Barone, F. Ando, et al., Chronic infiltrative lung diseases: value of gadolinium-enhanced MRI in the evaluation of disease activity-early report, Chest 117 (4) (2000) 1173–1178.
[36] N. Ogasawara, K. Suga, Y. Karino, N. Matsunaga, Perfusion characteristics of radiation-injured lung on Gd-DTPA-enhanced dynamic magnetic resonance imaging, Investig. Radiol. 37 (8) (2002) 448–457.
[37] K. Suga, N. Ogasaware, N. Matsunaga, K. Sasai, Perfusion characteristics of oleic acid–injured canine lung on Gd-DTPA–enhanced dynamic magnetic resonance imaging, Investig. Radiol. 36 (7) (2001) 386–400.
[38] R. Vij, M.E. Strek, Diagnosis and treatment of connective tissue disease-associated interstitial lung disease, Chest 143 (3) (2013) 814–824.
[39] S.C. Mathai, S.K. Danoff, Management of interstitial lung disease associated with connective tissue disease, BMJ 352 (2016) h6819.
[40] Y. Ohno, H. Koyama, T. Yoshikawa, S. Seki, State-of-the-art imaging of the lung for connective tissue disease (CTD), Curr. Rheumatol. Rep. 17 (12) (2015) 69.
[41] E.J. Kim, H.R. Collard, T.E. King Jr., Rheumatoid arthritis-associated interstitial lung disease: the relevance of histopathologic and radiographic pattern, Chest 136 (5) (2009) 1397–1405.
[42] Y. Ohno, M. Nishio, H. Koyama, D. Takenaka, M. Takahashi, T. Yoshikawa, et al., Pulmonary MR imaging with ultra-short TEs: utility for disease severity assessment of connective tissue disease patients, Eur. J. Radiol. 82 (8) (2013) 1359–1365.
[43] CdS. Müller, D. Warszawiak, EdS. Paiva, D.L. Escuissato, Pulmonary magnetic resonance imaging is similar to chest tomography in detecting inflammation in patients with systemic sclerosis, Rev. Bras. Reumatol. 57 (5) (2017) 419–424.
[44] I. Pinal-Fernandez, V. Pineda-Sanchez, E. Pallisa-Nuñez, C.P. Simeon-Aznar, A. Selva-O'Callaghan, V. Fonollosa-Pla, et al., Fast 1.5 T chest MRI for the assessment of interstitial lung disease extent secondary to systemic sclerosis, Clin. Rheumatol. 35 (9) (2016) 2339–2345.
[45] Y. Ohno, M. Nishio, H. Koyama, T. Yoshikawa, S. Matsumoto, S. Seki, et al., Oxygen-enhanced MRI for patients with connective tissue diseases: comparison with thin-section CT of capability for pulmonary functional and disease severity assessment, Eur. J. Radiol. 83 (2) (2014) 391–397.
[46] J.E. Kusmirek, M.D. Martin, J.P. Kanne, Imaging of idiopathic pulmonary fibrosis, Radiol. Clin. 54 (6) (2016) 997–1014.
[47] D.A. Lynch, N. Sverzellati, W.D. Travis, K.K. Brown, T.V. Colby, J.R. Galvin, et al.,

Diagnostic criteria for idiopathic pulmonary fibrosis: a Fleischner society white paper, The Lancet Respiratory Medicine, (2017).
[48] M.E. Kreider, J. Hansen-Flaschen, N.N. Ahmad, M.D. Rossman, L.R. Kaiser, J.C. Kucharczuk, et al., Complications of video-assisted thoracoscopic lung biopsy in patients with interstitial lung disease, Ann. Thorac. Surg. 83 (3) (2007) 1140–1144.
[49] C.J. Lettieri, G.R. Veerappan, D.L. Helman, C.R. Mulligan, A.F. Shorr, Outcomes and safety of surgical lung biopsy for interstitial lung disease, Chest 127 (5) (2005) 1600–1605.
[50] J.M. Wild, Imaging Pathophysiological Changes in the Lungs in IPF with Xenon Magnetic Resonance Imaging, BMJ Publishing Group Ltd, 2018.
[51] S.B. Fain, F.R. Korosec, J.H. Holmes, R. O'halloran, R.L. Sorkness, T.M. Grist, Functional lung imaging using hyperpolarized gas MRI, J. Magn. Reson. Imaging: Off. J. Int. Soc. Magnetic Res. Med. 25 (5) (2007) 910–923.
[52] J.E. Roos, H.P. McAdams, S.S. Kaushik, B. Driehuys, Hyperpolarized gas MR imaging: technique and applications, Magn. Reson. Imag. Clin. 23 (2) (2015) 217–229.
[53] D. Kramer, For some, helium-3 supply picture is brightening, Phys. Today 64 (5) (2011) 20.
[54] M. Kirby, L. Mathew, A. Wheatley, G.E. Santyr, D.G. McCormack, G. Parraga, Chronic obstructive pulmonary disease: longitudinal hyperpolarized 3He MR imaging, Radiology 256 (1) (2010) 280–289.
[55] A.J. Swift, J.M. Wild, S. Fichele, N. Woodhouse, S. Fleming, J. Waterhouse, et al., Emphysematous changes and normal variation in smokers and COPD patients using diffusion 3He MRI, Eur. J. Radiol. 54 (3) (2005) 352–358.
[56] R.P. Thomen, A. Sheshadri, J.D. Quirk, J. Kozlowski, H.D. Ellison, R.D. Szczesniak, et al., Regional ventilation changes in severe asthma after bronchial thermoplasty with 3He MR imaging and CT, Radiology 274 (1) (2014) 250–259.
[57] K. Qing, K. Ruppert, Y. Jiang, J.F. Mata, G.W. Miller, Y.M. Shim, et al., Regional mapping of gas uptake by blood and tissue in the human lung using hyperpolarized xenon-129 MRI, J. Magn. Reson. Imaging 39 (2) (2014) 346–359.
[58] S. Patz, I. Muradian, M.I. Hrovat, I.C. Ruset, G. Topulos, S.D. Covrig, et al., Human pulmonary imaging and spectroscopy with hyperpolarized 129Xe at 0.2 T, Acad. Radiol. 15 (6) (2008) 713–727.
[59] S.S. Kaushik, M.S. Freeman, S.W. Yoon, M.G. Liljeroth, J.V. Stiles, J.E. Roos, et al., Measuring diffusion limitation with a perfusion-limited gas—hyperpolarized 129Xe gas-transfer spectroscopy in patients with idiopathic pulmonary fibrosis, J. Appl. Physiol. 117 (6) (2014) 577–585.
[60] N.J. Stewart, G. Leung, G. Norquay, H. Marshall, J. Parra-Robles, P.S. Murphy, et al., Experimental validation of the hyperpolarized 129Xe chemical shift saturation recovery technique in healthy volunteers and subjects with interstitial lung disease, Magn. Reson. Med. 74 (1) (2015) 196–207.
[61] J.M. Wang, S.H. Robertson, Z. Wang, M. He, R.S. Virgincar, G.M. Schrank, et al., Using hyperpolarized 129Xe MRI to quantify regional gas transfer in idiopathic pulmonary fibrosis, Thorax 73 (1) (2018) 21–28.
[62] N.D. Weatherley, N.J. Stewart, H.-F. Chan, M. Austin, L.J. Smith, G. Collier, et al., Hyperpolarised xenon magnetic resonance spectroscopy for the longitudinal assessment of changes in gas diffusion in IPF, Thorax 74 (2019) 500–502 thoraxjnl-2018-211851.
[63] P. Ungprasert, E.M. Carmona, J.P. Utz, J.H. Ryu, C.S. Crowson, E.L. Matteson (Eds.), Epidemiology of Sarcoidosis 1946-2013: a Population-Based Study. Mayo Clinic Proceedings, Elsevier, 2016.
[64] E.V. Arkema, Y.C. Cozier, Epidemiology of sarcoidosis: current findings and future directions, Ther. Adv. Chronic Dis. 9 (11) (2018) 227–240.
[65] E.M. Carmona, S. Kalra, J.H. Ryu (Eds.), Pulmonary Sarcoidosis: Diagnosis and Treatment. Mayo Clinic Proceedings, Elsevier, 2016.
[66] J.H. Chung, B.P. Little, A.V. Forssen, J. Yong, A. Nambu, D. Kazlouski, et al., Proton MRI in the evaluation of pulmonary sarcoidosis: comparison to chest CT, Eur. J. Radiol. 82 (12) (2013) 2378–2385.
[67] A.S. Bhalla, A. Das, P. Naranje, A. Goyal, R. Guleria, G.C. Khilnani, Dilemma of diagnosing thoracic sarcoidosis in tuberculosis-endemic regions: an imaging-based approach. Part 2, Indian J. Radiol. Imaging 27 (4) (2017) 380.
[68] S.B. Gorkem, S. Köse, E.Y. Lee, S. Doğanay, A.S. Coskun, M. Köse, Thoracic MRI evaluation of sarcoidosis in children, Pediatr. Pulmonol. 52 (4) (2017) 494–499.
[69] D. Brady, L. Lavelle, S. McEvoy, D. Murphy, A. Gallagher, B. Gibney, et al., Assessing fibrosis in pulmonary sarcoidosis: late-enhanced MRI compared to anatomic HRCT imaging, QJM: Int. J. Med. 109 (4) (2015) 257–264.
[70] W. Luboldt, A. Wetter, K. Eichler, T. Vogl, T. Wagner, M. Seemann, Determination of the optimal MRI sequence for the detection of malignant lung nodules, Eur. J. Med. Res. 11 (8) (2006) 336.
[71] J.H. Chung, C.W. Cox, A.V. Forssen, J. Biederer, M. Puderbach, D.A. Lynch, The dark lymph node sign on magnetic resonance imaging: a novel finding in patients with sarcoidosis, J. Thorac. Imaging 29 (2) (2014) 125–129.